Use of a High-Throughput Screening Approach Coupled with *In Vivo* Zebrafish Embryo Screening To Develop Hazard Ranking for Engineered Nanomaterials

Saji George,[†,‡] Tian Xia,[†,‡] Robert Rallo,[‡,∥,∞] Yan Zhao,[¶] Zhaoxia Ji,[‡] Sijie Lin,[‡] Xiang Wang,[‡] Haiyuan Zhang,[‡] Bryan France,[§] David Schoenfeld,[‡,¶] Robert Damoiseaux,[‡,§] Rong Liu,[‡,∥] Shuo Lin,[¶] Kenneth A. Bradley,[‡,⊥] Yoram Cohen,[‡,∥] and André E Nel[†,‡,*]

[†]Department of Medicine, Division of NanoMedicine, [‡]Center for Environmental Implications of Nanotechnology, California NanoSystems Institute, [∞]Departament d'Enginyeria Informatica i Matematiques, Universitat Rovira i Virgili, Spain, [§]Molecular Shared Screening Resources, [⊥]Department of Microbiology, Immunology and Mol Genetics, [∥]Chemical and Biomolecular Engineering, and [¶]Department of Molecular, Cell, and Developmental Biology, University of California, Los Angeles, California 90095, United States

ABSTRACT Because of concerns about the safety of a growing number of engineered nanomaterials (ENM), it is necessary to develop high-throughput screening and *in silico* data transformation tools that can speed up *in vitro* hazard ranking. Here, we report the use of a multiparametric, automated screening assay that incorporates sublethal and lethal cellular injury responses to perform high-throughput analysis of a batch of commercial metal/metal oxide nanoparticles (NP) with the inclusion of a quantum dot (QD1). The responses chosen for tracking cellular injury through automated epifluorescence microscopy included ROS production, intracellular calcium flux, mitochondrial depolarization, and plasma membrane permeability. The z-score transformed high volume data set was used to construct heat maps for *in vitro* hazard ranking as well as showing the similarity patterns of NPs and response parameters through the use of self-organizing maps (SOM). Among the materials analyzed, QD1 and nano-ZnO showed the most prominent lethality, while Pt, Ag, SiO_2, Al_2O_3, and Au triggered sublethal effects but without cytotoxicity. In order to compare the *in vitro* with the *in vivo* response outcomes in zebrafish embryos, NPs were used to assess their impact on mortality rate, hatching rate, cardiac rate, and morphological defects. While QDs, ZnO, and Ag induced morphological abnormalities or interfered in embryo hatching, Pt and Ag exerted inhibitory effects on cardiac rate. Ag toxicity in zebrafish differed from the *in vitro* results, which is congruent with this material's designation as extremely dangerous in the environment. Interestingly, while toxicity in the initially selected QD formulation was due to a solvent (toluene), supplementary testing of additional QDs selections yielded *in vitro* hazard profiling that reflect the release of chalcogenides. In conclusion, the use of a high-throughput screening, *in silico* data handling and zebrafish testing may constitute a paradigm for rapid and integrated ENM toxicological screening.

KEYWORDS: nanotoxicology · hazard ranking · high-throughput screening · self-organizing map · zebrafish

The safety of engineered nanomaterials (ENM) is currently receiving a lot of attention, including how to perform hazard assessment of the large number of new materials that are emerging.[1] Currently, there are putatively more than 1000 consumer products that incorporate ENMs, and this number is expected to grow to 10^4 materials within a decade.[2] Thus, the sheer number of ENMs and their novel properties could overwhelm the traditional toxicological screening approaches that are used for chemicals, including the use of descriptive approaches in whole animals.[3,4] It is therefore appropriate that the National Research Council (2007) of the U.S. National Academy of Sciences proposed the use of more robust models for *in vitro* toxicological testing that can be carried out for larger batches of toxicants but still maintain relevance to *in vivo* outcomes.[5] There is an urgent need not only to adapt existing toxicological approaches for the screening of more than 60 000 industrial chemicals but also to use high-volume screening approaches for the safety evaluation of ENMs. One possible solution to overcome this bottleneck is high-throughput screening (HTS) that makes use of automated platforms to conduct assays and to generate data for *in vitro* and *in silico* based hazard ranking. HTS has the advantage of reduced reagent requirements, rapidity of analysis, reduced manpower needs, and providing a cost-effective screening approach that can also be used to prioritize materials for *in vivo* testing.

Recently, we have reported a rapid throughput method to test a small batch of in-house metal oxide nanoparticles (NPs) that were previously characterized for their ability to generate sublethal and lethal responses according to conventional screening assays in target cells.[6] This automated,

* Address correspondence to anel@mednet.ucla.edu.

Received for review October 12, 2010 and accepted January 26, 2011.

Published online February 16, 2011
10.1021/nn102734s

image-based epifluorescence procedure utilizes contemporaneous sublethal (*e.g.*, intracellular Ca^{2+} flux and mitochondrial perturbation) and lethal (cell death with increased membrane permeability) response outcomes. While this multiparametric assay was successful in distinguishing the toxicological profiles of TiO_2, CeO_2, and ZnO NPs, we have not utilized this system for hazard assessment of a large batch of unscreened commercial NPs. To implement such a high-throughput approach, it is necessary to develop computational and data transformation approaches to deal with the high volume data sets and perform hazard ranking for comparison to *in vivo* outcome. Ideally, the *in vivo* platform should have the built-in potential for high content screening that is commensurate with the *in vitro* test platform.

In this communication, we used our established multiparametric assay to develop HTS and *in silico* decision-making tools that can be used to compare *in vitro* hazard ranking to *in vivo* toxicological outcomes in zebrafish (*Danio rerio*) embryos. Zebrafish is as an appropriate *in vivo* model for comparative studies on mammalian biology[7] and has recently also been used to study NP toxicity and for developing HTS.[8−13] Although many independent studies have separately reported the physicochemical characterization of NPs and their toxicity under *in vitro* and *in vivo* conditions, relatively few studies have addressed these issues jointly. Moreover, among the limited studies carried out, only a few have shown correlations between *in vitro* and *in vivo* outcomes.[14−16] We demonstrate that it is possible to use the multiparametric assay in combination with computerized data analysis (heat maps and self-organizing maps) and zebrafish embryo screening to develop a parallel toxicological screening paradigm that provides proof-of-principle testing of how to speed up ENM hazard assessment.

RESULTS

NP Physical−Chemical Characterization and Dispersion in Tissue Culture Media. The suppliers and primary physical−chemical characteristics of nano-Ag, Au, Pt, Al_2O_3, SiO_2, ZnO, and QD1 are provided in Table S1 and Figure S1 in the Supporting Information. The choice of these materials was based on commercially available metal and metal oxides in a comparable size range as well as a QD (QD1) that have not previously been assessed for toxicological potential. Materials were randomly selected for proof-of-principal testing without an attempt to control their properties through a rigorous in-house synthesizes approach that we previously used to establish our multiparametric assay. Since the surface chemistry and state of dispersion affect NP bioavailability and biological activity, we attempted to obtain the best possible state of particle dispersion by initial suspension in deionized water followed by the addition of bovine serum albumin (BSA) and then transferring the suspension to bronchial epithelial growth medium (BEGM) or complete Dulbecco's modified Eagle's medium (CDMEM) (Figure S2).[17] BEGM and CDMEM are used for culturing bronchial epithelial (BEAS-2B) and macrophage (RAW 264.7) cell lines, respectively.[18] Table 1 shows the average particle sizes in aqueous media, demonstrating that particle stabilization with BSA and fetal bovine serum (FBS) improved dispersal, except for CdSe/ZnS (QD1). Determination of particle agglomeration kinetics by using a high-throughput dynamic light scattering (DLS) approach confirmed the stability of NP suspensions achieved by the addition of protein to the suspension medium (Figure S3). Generally, CDMEM (containing 10% FBS) resulted in agglomerate sizes <100 nm except for Al_2O_3 and SiO_2 (Figure S3). BSA provided the same effect in BEGM. Although agglomeration increased following 2 h incubation in CDMEM, the largest agglomerates retained hydrodynamic diameters <250 nm at 24 h, with the exception of SiO_2 (Figure S3). NP dispersal in tissue culture media resulted in a slightly more negative zeta-potential compared to the values in water (Table 1).

TABLE 1. Particle Size and Zeta-Potential Measurements[a]

	average agglomeration size (nm)			zeta-potential (mV)		
NPs	water	CDMEM	BEGM + BSA	water	CDMEM	BEGM + BSA
Ag	95.68	77.17	110	−0.7	−10.2	−8.77
Au	294.45	21.9	29.1	−7.4	−6.15	−1.93
Pt	271	28.6	173	−4.1	−9.26	−8.58
Al_2O_3	1168	25.8	57	−7.7	−10.6	−8.47
SiO_2	1135.35	341.5	528.3	−1.6	−6.54	−10.4
QD1	168.5	48.5	443.2	78.4	−10.3	−10.1
ZnO	130.5	24.23	45.17	17.4	−7.16	−7.93

[a] Agglomeration size and zeta-potential were assessed in 50 μg/mL NPs suspended in water and cell culture media as depicted in Figure S2 in the Supporting Information. Please notice the decrease in particle size in CDMEM compared to BEGM or water. The original zeta-potential values of NPs in water were masked upon suspension in cell culture media. CDMEM = complete Dulbecco's modified Eagle medium supplemented with 10% fetal bovine serum (FBS). BEGM = bronchial epithelial growth medium, supplemented with growth factors and 2 mg/mL BSA but no serum. In addition to average particle size characterization, we also studied other particle characteristics and agglomeration kinetics in different exposure media which are reported in Supporting Information. Values represent mean of three separate experiments, each including three replicates per group.

NP Hazard Ranking by the Performance of HTS and Generation of Heat Maps. While there are a wide range of possible toxicological responses to ENMs, we have developed a multiparametric cellular assay that utilizes an integrated set of response parameters that reflect the abilities of some types of ENMs to induce cytotoxicity through mechanisms that may involve oxygen radical generation and oxidative stress,[6] cationic injury,[19] and metal ion shedding.[18−20] The oxidative stress paradigm has proven useful for the *in vitro* hazard ranking of ENMs with electronically active surfaces (*e.g.*, semiconductor particles), particles with adsorbed transition metals or redox

cycling organic chemicals (*e.g.*, carbon nanotubes), ability to generate electron−hole pairs (through photoactivation, *e.g.*, TiO_2), or particle dissolution leading to shedding of toxic metal ions (*e.g.*, ZnO and chalcogenides).[1,21,22] Moreover, the set of interconnected responses being used in this assay (intracellular calcium flux, mitochondrial membrane depolarization, and membrane leakage) can also be triggered by ENM properties that secondary leads to the generation of oxidative stress, for example, as a result of mitochondrial damage.[18,19] Thus, our screening assay is capable of reflecting quite a wide range of ENM hazardous effects.

To test the ability of our assay to handle a large and randomly selected batch of commercial NPs, the screen was performed in 384-well plates to allow each particle to be assessed at multiple different concentrations and for different time periods (see plate layout in Figure S4 in Supporting Information). Following the incubation with the NPs for incremental lengths of time, three cocktails of compatible dyes were dispensed into the plates as shown in Figure S4. These dyes include Hoechst 33342 for nuclear staining and cellular localization, MitoSox Red to assess mitochondrial superoxide generation (ROS), JC1 to assess mitochondrial depolarization (MMP), Fluo-4 to detect a rise in intracellular calcium flux ($[Ca]_i$), and propidium iodide (PI) to assess surface membrane permeability.

After cellular exposure to the randomly selected NP batch (Ag, Au, Pt, Al_2O_3, SiO_2, ZnO, and QD1) at nine different doses and for eight different lengths of time, the epifluorescence readout was analyzed by MetaXpress software to score the percentage of positive responses. A positive response is defined as an increase in the fluorescence above the threshold for each dye as previously described by us.[6] The raw data were processed and normalized by robust *z*-score transform (as outlined in Materials and Methods) to correct for interplate variability and data comparability. Robust *z*-score was generated by subtracting the plate median from each of the individual raw values and then dividing the difference by the median absolute deviation for that particular plate. In the current analysis, a *z*-score value ≥ 3 represents a statistically significant increase ($p < 0.05$) in the number of positive cells for a particular response parameter. The robust *z*-score values were transformed into heat maps in which the rows and columns correspond to the dose and time response parameters for each NP, respectively. Heat maps were used to visually rank the high content data set. In this representation, blue colors indicate no harmful activity while yellow-red colors indicate incrementally more severe cellular responses. Map reading shows differential toxicity profiles for individual NP types (Figure 1). ZnO and QD1 induced mitochondrial ROS production in both cell types at different intensities (Figure 1). The same NPs were also capable of inducing increases in $[Ca^{2+}]_i$ flux, lowering of MMP and

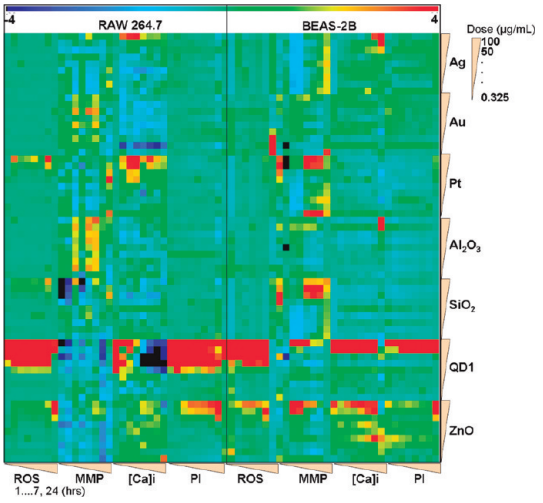

Figure 1. Heat map display of the HTS data. The raw data normalized by robust *z*-score transformation was used to develop the heat map, using MeV software. The rows and columns in the heat map correspond to the dose range and exposure times, respectively, in each cell type. Blue colors indicate no harmful activity, while yellow/red indicates a significant increase in cellular responsiveness. The responses are designated as follows: (i) ROS = measurement of mitochondrial superoxide generation measured by MitoSox Red, (ii) MMP = perturbation of mitochondrial membrane potential as measured by JC1, (iii) $[Ca]_i$ = increased intracellular Ca^{2+} flux measured by Fluo-4, (iv) PI = measurement of membrane permeability by propidium iodide uptake. QD1 and ZnO NPs generated a significant increase (values $\geq +3$) in robust *z*-scores in a dose- and time-dependent manner. These particles generated sublethal and lethal cellular responses. By contrast, Pt, Ag, SiO_2, Al_2O_3, and Au NPs generated sublethal effects only that are not accompanied by increased membrane permeability. These experiments were repeated three times with four replicates in each group. A complete description of the procedures and materials to conduct the HTS assay and data analysis appears in the Materials and Methods.

cytotoxicity (PI uptake). While Ag, Al_2O_3, Pt, Au, and SiO_2 NPs triggered sublethal responses, they did not increase PI uptake. By visual inspection of the heat map, we provisionally rank the toxicity of NPs as QD1 > ZnO > Pt > SiO_2 > Ag > Al_2O_3 = Au.

In order to compare the multiparametric to single response assays, we also measured cellular ATP levels (Figure 2a) and mitochondrial metabolic activity (MTS assay) (Figure 2b). While QD1 and ZnO were capable of reducing ATP levels and increasing MTS activity in accordance with their cytotoxic effects in the multiparametric assay, nano-Pt also showed reduction in ATP levels and MTS activity (Figure 2a,b). This raises the question as to whether nano-Pt may induce lethal effects because of different sensitivities of the single end point *versus* the multiparametric response approach. The remaining particles did not exert effects on ATP levels or MTS activity, except for a small decrease in ATP levels at a high dose of SiO_2. This could reflect a SiO_2 effect on mitochondrial function as confirmed by the MMP response in BEAS-2B cells (Figure 1) or may represent a false positive result due to the agglomeration of these particles, as seen in

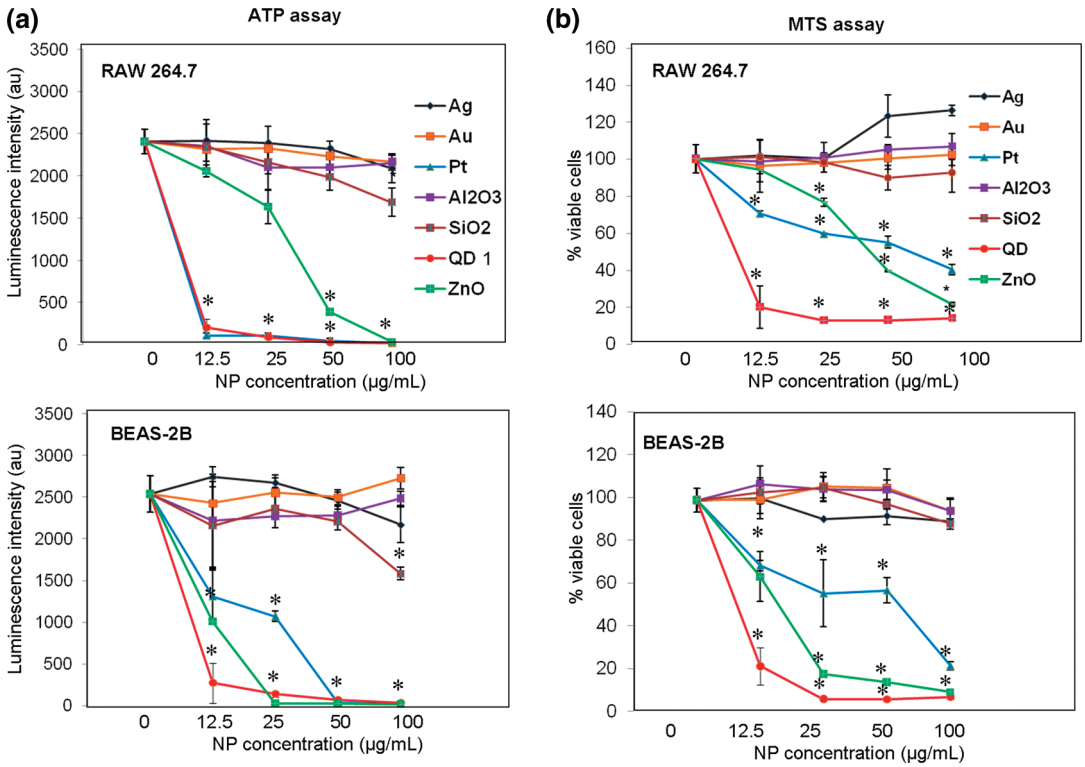

Figure 2. Single response assays for comparison to the HTS results. In order to identify potential false positive/negative results in the HTS assay, NPs were tested in traditional single parameter assays that reflect cellular ATP level and mitochondrial dehydrogenase activity (MTS assay). This adjunct screening confirmed the cytotoxicity of QD1 of ZnO. Noteworthy, nano-Pt also resulted in decreased ATP levels and a decrease in MTS activity, while SiO_2 showed a slight decrease in ATP levels at the highest dose. This could mean that Pt may be potentially cytotoxic and that the SiO_2 effects in the HTS assay could be either true mitochondrial perturbation or a false positive response due to the tendency of these particles to agglomerate at high doses. *Values statistically significant from control values ($p \leq 0.05$), where each experiment was conducted three times with three replicates in each group. Error bars represent standard deviation from average value.

TABLE 2. Source of QDs Used in This Study

QDs	supplier	formulation	purity	primary particle size (nm)
CdSe/ZnS (QD1)	Sigma Aldrich	dispersion in toluene		6.5
CdSe/ZnS (QD2)	NN Lab	surface capping with mercaptoundecanoic acid dispersed in water	99%, not including the ligand	7.5−8
CdSe (QD3)	NN Lab	surface capping with mercaptoundecanoic acid dispersed in water	99%, not including the ligand	6.5

Figure S3 in the Supporting Information. While these results show that data interpretation of *in vitro* tests needs to proceed with care, we prefer multiparametric testing because it provides sublethal and lethal response tracking and also allows additional response profiling that cannot be accomplished with single response assays (see below).

Analysis of the QD1 toxicity data was quite interesting. Inspection of the QD1 product sheet showed that these particles were suspended in toluene, and therefore, this product's toxicity may be unrelated to primary QD components. Since the presence of contaminants is a frequent concern in ENM toxicity assessment, we also studied toluene by itself and confirmed that this solvent could indeed generate a HTS toxicity profile identical to QD1 (data not shown). Therefore, to determine whether the chalcogenide and Zn compounds in other QD formulations may contribute to toxicity of this class of materials, we acquired two additional types of QDs that are commercially available and are toluene-free (Table 2). Moreover, we compared the new formulations for their ability to release chalcogenides and Zn as determined by ICP-MS. Thus, while QD2 (CdSe/ZnS particles with a core−shell structure) released little or no Cd, Se, or Zn, QD3 (CdSe particles without a shell or a Zn content) released more chalcogenide components (Figure 3a). Interestingly, QD3 was more toxic than QD2 but not nearly as toxic as the toluene-suspended particles (Figure 3b). This toxicity ranking was confirmed by performing MTS assay in BEAS-2B and RAW 264.7 cells (Figure 3c). Thus, without claiming that above selections are representative of all QDs, we demonstrate the importance of interpreting HTS with care, including relating ENM

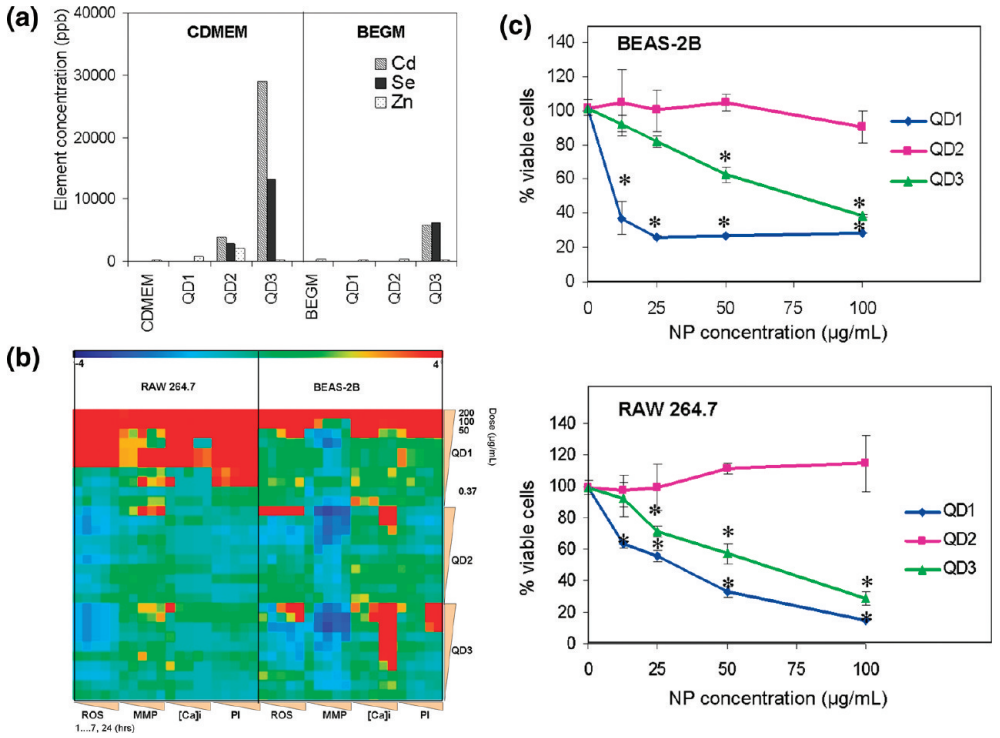

Figure 3. Evaluation of QD cytotoxicity due to differences in particle composition and tendency to shed chalcogenide ions. Three different QDs are being compared for their ability to induce toxicity in the HTS and MTS assays. These are (i) QD1, which is a core/shell CdSe/ZnS particle from Sigma prepared in toluene; (ii) QD2, which is a core/shell CdSe/ZnS particle stabilized by mercaptoundecanoic acid in water; (iii) QD3, which is a core CdSe particle stabilized by mercaptoundecanoic acid in water. (a) ICP-MS analysis. QDs suspended in CDMEM and BEGM media were subjected to ultracentrifugation after 24 h, and the supernatants were assayed for the presence of Cd, Se, and Zn by ICP-MS (Perkin-Elmer SCIEX Elan DRCII). (b) Heat map representation of robust *z*-score transformed multiparametric HTS data comparing dose- and time-dependent toxicity as described in Figure 1. The abbreviations for the cellular responses are the same as in Figure 1. (c) MTS-based cell viability assays in BEAS-2B and RAW 264.7 cells. The MTS assay was performed at increasing particle concentrations 24 h after their introduction. *Values statistically significant from control values ($p \leq 0.05$), where each experiment was conducted three times with three replicates in each group. Error bars represent standard deviation from average value.

composition and the possible presence of impurities to toxicological outcome. The screening exercise that we have begun in this communication now also needs to be extended to the wide range of QDs being produced in the market place. This will be particularly important for the safety assessment of QDs that are being developed for *in vivo* applications or may be included in products that could come into contact with humans and the environment.

Data Analysis To Show Linkage between the Toxicological Response Characteristics through the Use of Self-Organizing Maps (SOMs). The multidimensional data set generated by our primary HTS analysis (Figure 1) includes 4032 data points (2 cell lines × 4 cytotoxicity responses × 8 time points × 7 NPs × 9 doses) that may include hidden or non-obvious relationships between variables such as material type, dose kinetics, response, and cell type. We used SOM analysis to project the HTS data set onto a two-dimensional display wherein the spatial distribution of the different NPs at given concentrations provide a qualitative indicator of the degree of similarities or differences between materials that generate one or more of the cellular response outcomes (Figure 4a). Shorter distances over the SOM projection are indicative of underlying similarities in the NPs' activity profiles (Figure 4a). Four clusters of NPs were identified based on the similarities between their lethal response outcomes (C1−C4). Cluster C1 consists of toxic QD1 (or more appropriately its toluene content) and ZnO at indicated doses in brackets. Cluster C2 consists of lower doses (0.3−50 μg/mL) of ZnO and high doses (50−100 μg/mL) of Ag NPs, while cluster 3 includes moderately toxic NPs (Pt and SiO_2). Cluster 4 comprises noncytotoxic NPs (Au, Al_2O_3) or ineffective doses of potentially cytotoxic NPs. Please notice that in Figure 4a each of the SOM clusters contains SOM units (or subclusters) whose relative spacings are indicative of the degree of similarity. Thus, SOM units that are closer to one another are more similar with respect to toxicity profiles, as illustrated by clustering of different ZnO concentrations in cluster C2. Moreover, C2 also contains high doses of Ag and a low dose QD1 SOM unit (Figure 4a). It is interesting to note that clusters 1 and 2 consisted primarily of highly cytotoxic ZnO and QD1, while cluster C4 is more heterogeneous and includes Ag, Pt, SiO_2, Au, and Al_2O_3.

The HTS data set was also clustered to find SOMs that show relatedness between the cytotoxic response profiles of each cell type (Figure 4b). Four clusters emerged from this analysis. Cluster C1 grouped mostly RAW 264.7

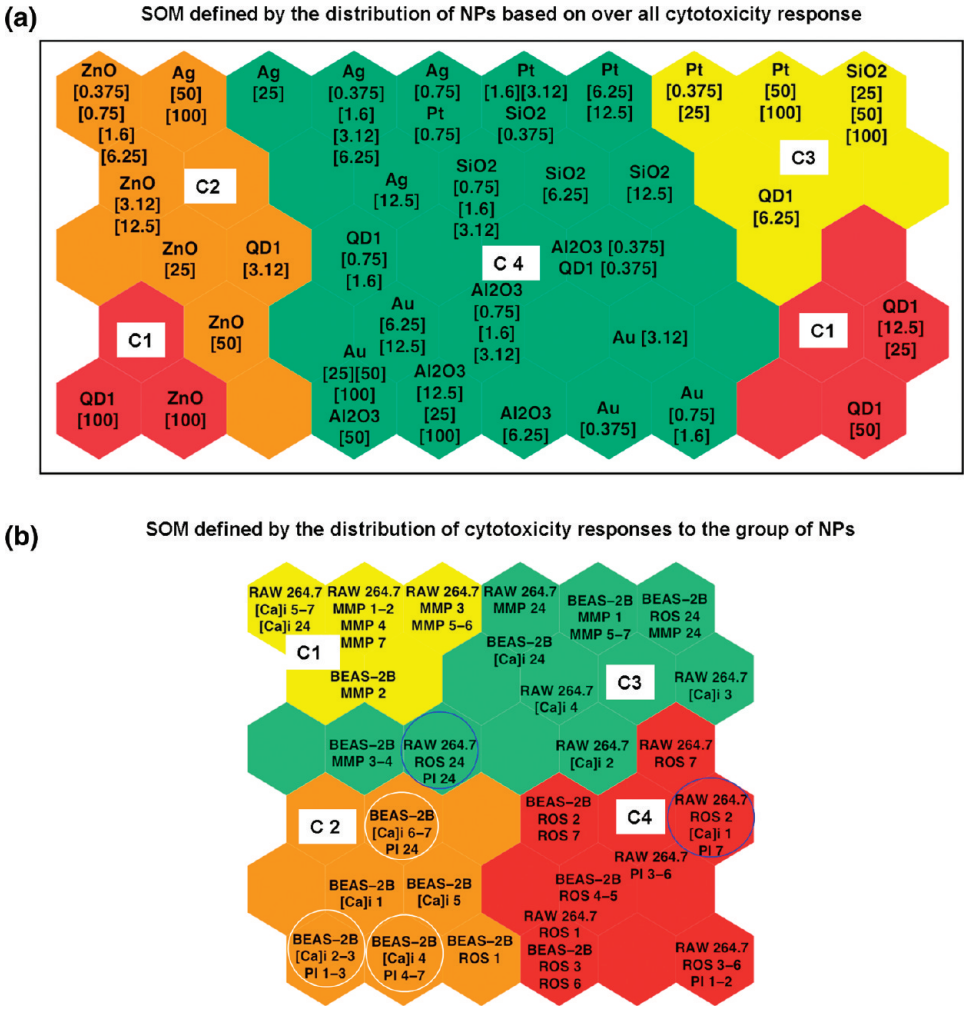

Figure 4. Use of SOMs to identify similarity patterns for NPs and cellular responses. (a) SOM defined by the distribution of NPs on a 2D grid that considers all response characteristics in both cell types. This SOM is generated by the integration of the entire data set to distribute NPs based on the biological response measurements. NPs showing similarity in their cytotoxicity responses cluster together. Noteworthy is the clustering of highly toxic NPs (ZnO and QD1) at moderate to high concentrations in clusters C1 and C2, while cluster C3 comprises Pt and SiO_2, with cluster 4 incorporating most noncytotoxic NPs. (b) SOM defined by the clustering of the various biological response parameters. This SOM is generated by integrating the entire data set to distribute the cellular responses to the entire set of NPs. Four clusters emerged from the analysis of the distribution of the various biological response parameters. Cluster C1 grouped mostly RAW 264.7 intracellular calcium flux and mitochondrial membrane depolarization. Cluster C2 grouped BEAS-2B calcium flux and PI uptake exclusively.

cellular responses that track intracellular calcium flux and MMP dissipation. Cluster C2 relates exclusively to BEAS-2B cellular responses, including intracellular calcium flux and membrane permeability (Figure 4b). Noteworthy is the grouping of intracellular calcium flux with PI uptake in the lower subclusters in BEAS-2B cells (white circles in Figure 4b). In contrast, the lower subclusters in RAW 264.7 cells include a grouping of PI uptake and mitochondrial ROS responses (blue circle in Figure 4b), indicating a high degree of similarity in their induction profiles. Since the above results demonstrate overlap as well as differences between above cell lines, we also constructed a Pearson correlation matrix to delineate similarities and divergences between the RAW 264.7 and BEAS-2B cells. In brief, the results show cell-specific correlation between different response characteristics as outlined in the online data discussion (Figure S5 in Supporting Information).

Comparison of the *In Vitro* Toxicological Observation with *In Vivo* Data Generation in Zebrafish Embryos. In order to compare the cellular HTS results with *in vivo* outcome, we used the zebrafish (*Danio rerio*), which has been used as a model organism to screen for chemical and NP toxicity.[12,13,23] Zebrafish embryos exposed to NP suspensions at 4 h post-fertilization (hpf) were assessed for toxicity every 24 h, starting at 24 hpf and continuing for a 120 h observation period. To perform this analysis, it was necessary to obtain adequate NP dispersal in Holtfreter's medium, using a dispersion approach similar to that used for tissue culture media (Figure S2). The key difference from the particle suspension in tissue culture media is the use of alginate as

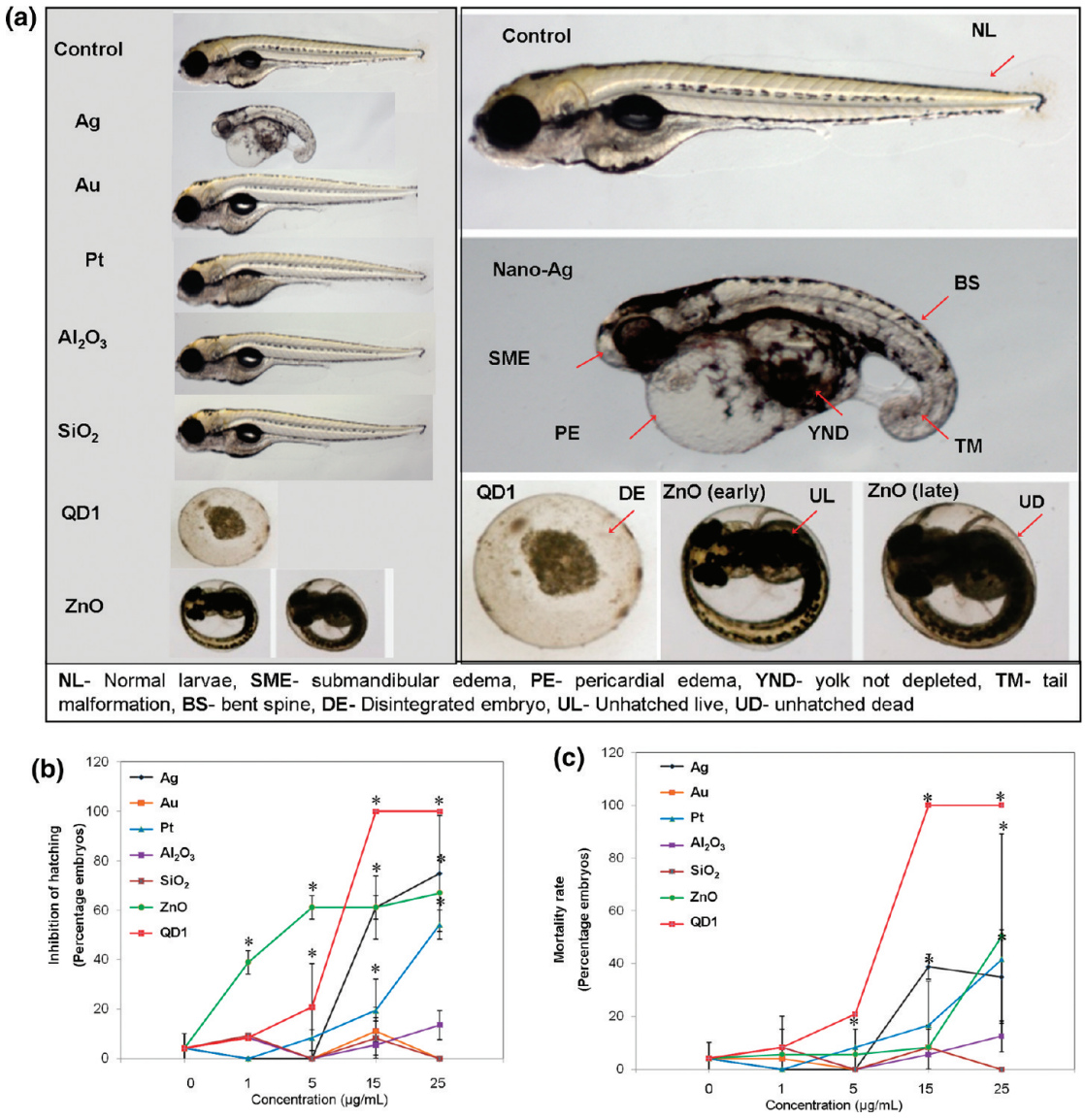

Figure 5. NP toxicity in zebrafish embryos. (a) Images of the zebrafish embryos exposed to Holtfreter's medium with and without the NPs added at 15 μg/mL for 72 hpf. Note the gross morphological defects seen in nano-Ag-treated embryos. The QD1 treatment resulted in the disintegration of embryo, while ZnO treatment inhibited embryo hatching. Zebrafish embryos exposed to increasing doses of NPs were also assessed for (b) the hatching rate at 72 hpf and (c) the mortality rate at 120 hpf. The average value was calculated for a total of 36 embryos from three experiments with 12 embryos in each group. *Values statistically significant from control ($p \leq 0.05$). Error bars represent standard deviation from average value.

a biologically relevant dispersant found in natural environmental waters (Figure S2).[24] High-throughput DLS analysis confirmed the reduction in NP agglomeration size and the improved stability through the inclusion of alginate in Holtfreter's medium (Figure S6). Toxicity end points involved scoring of hatching rates, mortality rates, cardiac rate, and the appearance of abnormal morphological features (*e.g.*, pericardial/yolk sac edema, large/small yolk, short tail, body length, bent spine, *etc.*). This analysis showed that QD1, ZnO, and Ag exert morphological effects, while Ag and Pt influenced the cardiac rate (Figures 5 and S7). Figure 5a demonstrates that nano-Ag-treated embryos develop bent spines, short body sizes, pericardial edema, submandibular edema, and bent tails by 120 h, while the majority of ZnO-treated embryos remained unhatched and embryos treated with QD1 died early and underwent complete dissolution within 24 h. ZnO consistently inhibited embryo hatching at all concentrations tested, while Ag and Pt NPs exerted effects on hatching at 15 and 25 μg/mL, respectively (Figure 5b). While toluene containing QD1 exerted high lethality at concentrations >5 μg/mL, ZnO and Pt induced sublethal responses that became lethal at 25 μg/mL (Figure 5c). Embryos treated with Ag and Pt NPs demonstrated a significant decrease in their cardiac rate at the sublethal dose of 15 μg/mL (Figure S7). Other particles (with the exception of the QD1) failed to affect cardiac rate. Exposure to Au, Al_2O_3, Fe_3O_4, and SiO_2 NPs did not affect the survival rate or morphology of zebrafish embryos (Figure 5b,c). Utilizing a scoring system for zebrafish

TABLE 3. Ranking of NPs Based on the Toxicity End Points in Zebrafish Embryos

ranking	attributes	NPs	morphological defects	physiological defects
0	no morphological or physiological defects	Au, Al_2O_3, SiO_2	no observable morphological defects	no physiological defects
1	single morphological/physiological defect			
2	multiple morphological and physiological defects	Pt, QD2	pericardial edema	low heart beat, mortality
3	severe multiple morphological and physiological defects	Ag, QD3	bent spine, opaque yolk, pericardial edema, yolk not depleted, short body, submandibular edema, tail malformation	mortality and reduced hatching rate and low heart beat
4	embryos do not survive	ZnO, QD1	unhatched embryo, disintegrated embryo	embryos do not survive, embryos fail to hatch

embryo toxicity, we were able to obtain an *in vivo* toxicological profile (Table 3). This demonstrated that Au, Al_2O_3, and SiO_2 attained a score of 0, Pt had a score of 2, Ag a score of 3, while ZnO and the QD1 each achieved a score of 4 (Table 3). Thus, while the *in vivo* profiling shows good agreement with the HTS assay, nano-Ag is clearly more toxic in zebrafish embryos than in mammalian cells. This likely relates to species' differences in the handling of Ag as will be discussed later on.

Because of the toxicological differences between different QD formulations in the secondary HTS screen (Figure 3c), we also compared QD2 and QD3 in our zebrafish embryo assay system. While QD2 had little effect on the survival and development of zebrafish embryos, QD3 induced a dose-dependent decrease in cardiac rate and hatching rate and an increase in mortality rate (Figure S8).

DISCUSSION

In this communication, we demonstrate that it is possible to apply our rapid-throughput toward a high-throughput screening (HTS) approach to assess commercially available NPs that were randomly chosen for comparison of their cytotoxic potential. This allowed us to obtain proof-of-principle testing for seven commercially acquired random NPs that were tested at multiple doses and different durations of time. We further demonstrate that how state-of-the-art *in silico* statistical approaches can transform the epifluorescence data into heat maps that are useful for hazard ranking as well as SOMs that explore similarities and differences between materials and cell types. The HTS assay demonstrated that a toluene-containing NP and ZnO NPs induced mitochondrial superoxide generation, $[Ca^{2+}]_i$ flux, and mitochondrial depolarization in cells that ultimately undergo cell death, while Pt, Ag, SiO_2, Au, and Al_2O_3 NPs induced sublethal effects without cell death. While these data showed good correlation to single response assays, Pt induced a decline in ATP levels and MTS activity that was not reflected by PI uptake in the HTS assay. We also compared the *in vitro* HTS results to the injurious effects of the NPs in zebrafish embryos, which showed the same hazard profiling except that nano-Ag was clearly more toxic in the embryos than in mammalian cells. This agrees with the notion that Ag poses extreme danger in the environment but is less toxic to humans.[25] Thus, through the use of an integrated cellular response pathway for screening, advanced *in silico* data analysis tools, and zebrafish embryo screening, it is possible to develop a predictive toxicological paradigm for ENM hazard assessment.

HTS offers the advantage of screening large NP batches as a first step towards ENM hazard assessment. Not only does this allow more rapid screening, but it also enables multiparameter assessment of lethal and sublethal responses. Because these multidimensional data sets are also useful for investigation of structure–activity and activity–activity relationships, we prefer multiparametric above single-response testing for hazard ranking. However, our study demonstrates that, when using HTS analysis, it is important to critically interpret the actual meaning of the data and be aware of potential pitfalls such as false positive results following optical interference by NP agglomeration or distinguishing between primary material effects and the influence of impurities, stabilizing agents, or solvents. Biologically relevant dispersing agents (BSA for cellular studies and alginate for zebrafish studies) allowed us to achieve the best possible NP dispersion in our HTS and zebrafish studies. This avoids the fluctuation in NP dose and increasing the signal-to-noise ratio. Awareness of the potential contribution of nonprimary particle additives or contaminants such as toluene was illustrated by the QD1 analysis, which prompted proof-of-principle testing of the fate of this solvent *versus* primary particle components toward QD toxicity. Thus, QD toxicity has to consider the primary chalcogenide components (Cd, Se), the presence of Zn in some formulations, the dissolution characteristics of the core–shell or core-only compositions, as well as presence of solvents. In this study, the core–shell structure of QD2 was associated with less metal shedding and toxicity than the QD3, which was composed of core alone (Figure 3, Figure S8D,E in Supporting Information). Thus, our HTS platform is capable of discerning a variety of components that may contribute toward QD toxicity but needs additional analysis such as ICP-MS to identify chemicals that may play a role in toxicity. Since QDs represent an important class of ENM with

industrial and biological applications other than imaging, further studies are warranted to delineate the possible range of injury mechanisms and design features that could lead to hazard reduction. We propose the use of a high-throughput screening platform to analyze QDs' risk-to-benefit ratio as well as for their possible safe design.

The cellular responses being tracked in our HTS assay are premised on previous studies showing that redox-active NPs can generate interlinked oxidative stress responses, which at the highest level (aka the third tier of the hierarchical oxidative stress response) can trigger $[Ca^{2+}]_i$ flux, mitochondrial depolarization, mitochondrial superoxide production, and cytotoxicity identified by increased PI uptake.[1,6,20] However, it is important to clarify that the individual or integrated response parameters could also be triggered by non-oxidant mechanisms, including toxicological pathways where ROS generation may be a secondary response (*e.g.*, mitochondrial injury) or alternative mechanisms that lead to the generation of intracellular calcium flux and mitochondrial injury.[26,27] Thus, while the initial parameters in our assay originated from an oxidative stress perspective, we have come to recognize that the same parameters capture afferent injury pathways that may not necessarily reflect a primary oxidant mechanism. The mechanisms by which Zn, toluene, Pt, Cd, and Se engage one or more of the multiparametric responses may help to refine and further improve this assay. Nano-ZnO is known to trigger pro-inflammatory and cytotoxic effects due to particle dissolution and Zn^{2+} shedding, which is associated with or leads to lysosomal damage, triggering of intracellular $[Ca^{2+}]_i$ flux, mitochondrial perturbation, and cytotoxicity.[6,18] While the current platform captures the cytotoxic events taking place at the highest tier of oxidative stress (tier 3) in addition to capturing afferent mechanisms that can lead to mitochondrial injury, ROS production, and intracellular calcium flux, our future HTS development could also cover pro-inflammatory responses, signal pathway activation, cell membrane damage, and other cellular stress responses. It is likely that a comprehensive series of biological assays will be required to cover the wide range of ENMs being developed.

Toluene has been shown to pose an occupational hazard to the central nervous system,[28] and in a rat study, toluene has been shown to induce ROS generation in the brain.[29] While oxidative stress generation could explain the toluene effect in our assay, we also need to consider that toluene can permeabilize mitochondrial and cell surface membranes.[30] Although toluene is not a primary ENM component, it is important to consider its use as a solvent in some classes of nanomaterials as well as considering that under real-world conditions a variety of toxic organics could chemisorb to the NP surfaces and may therefore show up in toxicological assays. While inorganic Pt compounds (*e.g.*, cisplatin) are reported to exert cytotoxic effects due to DNA damage caused by Pt(II),[31,32] nano-Pt has not been shown to induce oxidative stress and toxicity *in vitro* and *in vivo*.[33] However, it has been shown that Pt ions can accumulate in mitochondria as revealed by cisplatin toxicity studies in rats.[34] This agrees with our observation that washing of the nano-Pt could reduce its cytotoxicity (Figure S9). Several studies highlight the role of Cd ions in the cytotoxicity of QDs.[35−37] Cd is known to induce oxidative stress and to accumulate in mitochondria.[35,38] Moreover, a recent study demonstrated that coating of a CdSe core with a ZnS shell decreases particle toxicity by a factor of 10 due to the reduced Cd release.[35] However, use of this strategy for long-term protective effects is speculative because of the possible corrosion of the ZnS shell under acidifying intracellular conditions or in the environment.[36,37] It is also possible that the presence of Zn could perturb toxicological responses to the chalcogenide components. With respect to nano-Ag, we have observed comparatively minor triggering of $[Ca^{2+}]_i$ flux, which is in agreement with its low toxicity in humans and animals.[39,40] Although Ag^+ release by nano-Ag can induce oxidative stress through glutathione depletion,[41] the possibility of reaching a toxicity threshold in mammalians is reduced by the complexation of Ag^+ ions by sulfur-containing amino acids and proteins.[42]

In order to determine whether the HTS results correlate with the *in vivo* toxicity, we chose zebrafish embryos from the perspective that this organism allows comparative toxicity with mammalian systems and also has the potential to become a high-throughput platform.[10,43] Moreover, zebrafish has also been proposed as a model vertebrate for investigating chemical toxicity and has recently also been employed in studies of ENM toxicity, including demonstrating the toxicological effects of metal and metal oxide NPs.[11−13,23,44] When comparing the toxicological outcomes in the zebrafish embryos, we noticed important similarities to the cellular HTS results. While toluene could account for the zebrafish embryo toxicity of QD1, the release of Cd and Se from the uncapped particle (QD3) could also contribute to QD toxicity (Figure S8D,E). This is supported by the fact that QD2 with similar core composition and size failed to elicit any developmental impairment in zebrafish embryos. Our results concur with earlier studies showing the protective effect of ZnS capping.[13,37] However, while the toluene-containing QD1, QD3, ZnO, and Pt clearly had significant effects on embryo survival and cytotoxicity, a major difference was that nano-Ag was highly toxic in fish embryos but had little effect in mammalian cells (Figure 1 and Figure 5). Unlike the mammalian system, Ag^+ is an ionoregulatory toxicant in fish, where noncompetitive inhibition of the gill epithelial Na^+/K^- pump reduces active uptake of Na^+ and Cl^-.[45] This leads to a net loss of ions from blood plasma, resulting in circulatory failure and death of the fish.[45] Currently, we are developing cell line models of zebrafish to

avoid the difficulty in data interpretation arising from the species' level differences in tolerance to metal and metal oxide NPs.

While interspecies differences may preclude a direct mechanistic extrapolation from a mammalian cell to a fish embryo for nano-Ag, all of the other materials showed good concurrence between *in vitro* and *in vivo* testing. This includes nano-ZnO, which is regarded as extremely toxic in the environment, including inhibition of hatching, leading to embryo starvation and ultimate death. Although we attempted to show ROS production in intact zebrafish embryos utilizing fluorescent dyes, we did not succeed due to technical difficulties. However, we cannot exclude such a possibility because there is clear evidence in the rodent lung and in metal fume fever in humans that ZnO can induce oxidative stress.[46,47] We do have preliminary evidence, however, that Zn^{2+} can interfere in the function of a zebrafish hatching enzyme.[48] Interestingly, it has previously been reported that Pt ions can suppress the cardiac rate in zebrafish embryos,[49] which agrees with our findings.

While a robust *z*-score normalization of our HTS data set provided heat maps for NP hazard ranking (Figure 1), the SOM[50] feature is quite useful for finding similarity patterns among materials, cells, and cellular responses. This is equivalent to cluster analysis for microarray data.[51−53] Our SOM analysis could identify NP clusters that elicit similar responses as well as identifying positive correlations between individual response parameters in the individual cell types (Figure 4a,b). Thus, SOM analysis provides the opportunity to identify and select cell types to be included in HTS analysis. Further, as evidenced by the correlation matrix data, there is a strong correlation between mitochondrial superoxide generation, intracellular calcium flux, and PI uptake (Figure S5 in Supporting Information). This shows that the SOM analysis tool is capable of recognizing activity−activity relationships that can help to further refine HTS assay development.

CONCLUSION

The main objective of our study was to transform a rapid-throughput assay for ENM toxicity into a high-throughput platform that can be used for hazard identification and making predictions about the *in vivo* toxicological outcomes. We demonstrate that it is possible *to* use our multiparametric assay in high-throughput mode to identify hazard and activity−activity relationships through linkage to *in silico* analysis tools. We also demonstrate that it is possible to compare *in vitro* hazard ranking to toxicological outcomes in zebrafish embryos, with the exception of nano-Ag that was more toxic in embryos than in the mammalian cells.

MATERIALS AND METHODS

NP Sources and Preparation for Biological Experimentation. Spherical Ag, Au, Pt, Al_2O_3, SiO_2, and ZnO NPs of approximate 10 nm size were purchased from Meliorum Nanotechnologies (Rochester, NY). CdSe/ZnS quantum dot (LumiDot) dispersed in toluene (QD1) was purchased from Sigma Aldrich (St. Louis, MO). Water-soluble core/shell CdSe/ZnS (QD2) and core-only CdSe (QD3) particles with mercaptoundecanoic acid (MUA) surface modification were purchased from NN Laboratories (Fayetteville, AR) (see Table S1 and Table 2 for details). Working solutions of these NPs were prepared in bronchial epithelial growth medium (BEGM) (Lonza, San Diego, CA) and complete Dulbecco's modified Eagle's medium (CDMEM) (Invitrogen, Carlsbad, CA). Dry powder NPs (Ag, Au, Pt, Al_2O_3, SiO_2, and ZnO) were weighed and added to deionized water at a concentration of 5 mg/mL to make up the stock solutions. These solutions were subjected to water bath ultrasonication (3 W) and aliquoted to prepare working solutions. Twenty microliters of 4% bovine serum albumin (BSA) (Fraction −V; Gemini Bioproducts, USA) was added to an equal volume of each of the stock suspensions and allowed to equilibrate for 30 min at room temperature. One milliliter of CDMEM (complete DMEM containing 10% FBS) or 1 mL of BEGM (supplemented with 2 mg/mL BSA) was added to the BSA-stabilized NP suspensions before sonication for 15 s using a probe sonicator (VibraCell, Sonics, CT) at 30 W.[17] The scheme for preparing a NP suspension in tissue culture medium is shown in Figure S2 of the Supporting Information, and assessment of suspension stability is displayed in Figure S3.

For zebrafish experiments, we used Holtfreter's medium which contains 3.5 g of NaCl, 0.20 g of $NaCO_3$, 0.05 g of KCl, and 0.12 g of $CaCl_2$ dihydrate in 1000 mL of deionized water, pH 6.5−7. The filtered solution was supplemented with alginic acid (Sigma Aldrich) at a concentration of 100 ppm. Alginate was chosen as an environmentally relevant stabilizing agent. Aliquoted NP stock solutions were added to the Holtfreter's medium supplemented with alginate at a range of concentrations (6.25, 12.5, 25, and 50 μg/mL) and sonicated for 15 s using a probe sonicator. The scheme for preparing the NPs in Holtfreter's medium is shown in Figure S2, and the suspension stability is displayed in Figure S6.

Agglomerate Size Distribution and Zeta-Potential Measurement. Particle size distribution and their state of agglomeration/dispersion in tissue culture media as well in Holtfreter's were determined by high-throughput dynamic light scattering (HT-DLS, Dynapro Plate Reader, Wyatt Technology), as detailed by Ji *et al.* (Figure S2).[17] Assessment of the agglomeration kinetics (suspension stability) of the NP in tissue culture and Holtfreter's medium was done in standard 384-well plates, using the built-in kinetics feature of the HT-DLS instrument. Zeta-potential was assessed in a ZetaSizer Nano (Malvern Instruments, Westborough, MA) that measured the electrophoretic mobility of NP suspensions in CDMEM, BEGM plus 2 mg/mL BSA, or Holtfreter's medium plus alginic acid. Electrophoretic mobility was transformed into zeta-potential using the Helmholtz−Smoluchowski equation. Average values were calculated for three separate experiments each containing three replicates in each group.

Cell Culture and Co-incubation with NPs. Considering the potential of exposure to airborne nanomaterials *via* inhalation, we chose a human lung epithelial cell line (BEAS-2B) and a rat alveolar macrophage cell line (RAW 264.7) as cellular models for this study. The cells have also been used previously to establish our multiparametric assay[6] and are currently being used to implement HTS, while alternative cell types, including primary cells, are being investigated for inclusion in the future. All cell cultures were maintained in 25 cm^2 culture flasks, in which the cells were passaged daily at 70−80% confluency for RAW 264.7 and at similar density every 4 days for BEAS-2B cells. Recently thawed RAW 264.7 cells (ATCC# TIB71) were cultured in DMEM containing 10% FBS, 100 U/mL penicillin, 100 μg/mL streptomycin, and 2 mM L-glutamine (complete medium).[18] These cells

were plated at 5000 cells per well into 384-well plates (Greiner bio-one, NC, USA). Cells were cultured overnight at 37 °C in a 5% CO_2 incubator before NP treatment. BEAS-2B (ATCC# CRL-9609) cells were cultured in BEGM in type-I rat tail collagen-coated flasks (Corning Inc., MA, USA). Trypsinized cells were washed and plated at 5000 cells per well (in 50 μL) into 384-well plates. Cells were cultured for 2 days at 37 °C in a 5% CO_2 incubator before the addition of NPs. NPs prior coated with BSA and then dispersed in CDMEM or BEGM supplemented with 2 mg/mL BSA were used to treat RAW 264.7 and BEAS-2B cells, respectively. NP exposures were carried out at nine incremental doubling doses ranging from 0.375 to 100 μg/mL, as well as eight exposure times ranging from 1 to 7 and then 24 h. The layout of the 384-well plates is shown in Figure S4. This work was carried out in the California NanoSystems Institute (CNSI) using its automated HTS facility where cellular seeding of the plates, preparation of NP working solutions, NP additions to the wells, preparation and addition of fluorescence dyes were carried out with automated liquid handling devices. The instruments used in these automated tasks include a Multidrop (Thermo-Fischer, Waltham, MA) to facilitate faster addition of microliter reagent quantities to the 384-well plates, Precision 2000 (Biotek Instruments, Winooski, VT) for preparing doubling concentrations of NPs and Hydra 96 (Robbins Scientific, Golden Valley, MN) for transferring NP working concentrations to the cells.

Cellular Staining with Fluorescent Probes and High Content Epifluorescence Microscopy. Three cocktails of fluorescent probe (dye) mixtures were prepared by mixing wavelength-compatible dyes (Molecular Probes, Invitrogen, Carlsbad, CA) in DMEM media (Table S2 and Figure S4). DMEM medium devoid of phenol red was used to make the dye cocktails to avoid its possible interference with the fluorescence readout. The first cocktail contained Hoechst 33342 (1 μM) and MitoSox Red (5 μM). The second cocktail comprised Hoechst 33342 (1 μM) and JC1 (1 μM), while the third cocktail contained Hoechst 33342 (1 μM), Fluo-4 (5 μM), and propidium iodide (5 μM). A multidrop was used to add these dyes to the 384-well plates containing live cells. The utility of these dyes for tracking multiparameter cellular responses are summarized in Table S2. Twenty-five microliters of dye mixture was added to each well in the multiwell plate according to the plate layout shown in Figure S4 and incubated for 30 min under standard culture conditions in the dark. Fluorescence images of the cells from each well in the plate were captured hourly for 1−7 h and again after 24 h exposure using an automated epifluorescence microscope, Image-Xpress^{micro} (Molecular Devices, Sunnyvale, CA) equipped with laser autofocus. Images were collected using DAPI, FITC, and TRITC filter/dichroic combinations to image Hoechst 33342 (blue), JC1/Fluo-4 (green), and MitoSox/PI (red), respectively, under a 10× magnification.

The microscopic images were automatically analyzed by Meta-Xpress software. First, the images were "segmented" into subcellular structures (nucleus and cytoplasm) based on morphological features such as object size and fluorescence distribution. Images to assess total cell number and PI uptake were taken from the nuclear segment, while assessment of mitochondrial responses and Ca^{2+} levels were taken from the cytoplasmic segment. The total number of nuclei was counted using the following thresholds in the Hoechst/DAPI channel: approximate minimum width was 3 μm (about 3 pixels) and the approximate maximum width was 10 μm (about 7 pixels). The threshold intensity above background level was 100 gray levels. For the green and red channels, the approximate minimum width was 5 μm (about 6 pixels) and the approximate maximum width was 30 μm (about 22 pixels). The intensities above background were set at 250 and 500 gray levels, respectively. The percent of cells positive for a given cellular response (*e.g.*, PI uptake) was calculated based on the total cell number (Hoechst 33342 positive cells). The experiment was repeated three times with four replicates in each group.

In contrast to small molecules, several unique NP properties such as high adsorption capacity, optical properties, surface catalytic activity, *etc.*, can interfere with the fluorescence readout and may therefore introduce aberrant results.[54] We addressed these issues by incorporating adequate controls (NPs added to the dyes in the absence of cells, NPs with cells but without the addition of dyes, adding dyes to cells in the absence of NPs, *etc.*) as well as performing complementary experiments that assess cellular ATP content through a luminescence technique or metabolic activity (MTS assay) by an absorbance method.

ATP and MTS Assays. Cells grown in 96-well plates were treated with NPs at incremental doses (12.5, 25, 50, and 100 μg/mL) for 24 h. The plates were washed (3×) in PBS, and 25 μL/well of ATPLite (Perkin-Elmer, MA, USA) mixture was added. After 10 min, the plates were placed on a microwell plate reader (Spectramax M5^e, Molecular Devices, Sunnyvale, CA), shaken for 5 s, and the luminescence intensity was recorded. Each experiment was repeated on three separate occasions with three replicates in each group. For the MTS assay, the NPs were added to 96-well plates containing cells and received MTS solution (20 μL/well) after 24 h. After incubation for a further 3 h, the plates were placed on a microwell plate reader, shaken for 5 s, and the absorbance of the formazan product read at 492 nm. These experiments were repeated three times with three replicates in each group.

ICP-MS Analysis. ICP-MS analysis was performed to detect heavy metal release from QDs suspended in cell culture media. QDs (100 μg/mL) were suspended in 1 mL of culture medium (CDMEM and BEGM) for 24 h before the particles were spun down at 100 000g for 4 h and the supernatant collected. A 500 μL portion of supernatant was acidified with 500 μL of 7% ultrahigh purity nitric acid and the metal ion concentration measured by inductively coupled plasma mass spectrometry (ICP-MS) using a Perkin-Elmer SCIEX Elan DRCII. The average value is calculated from three replicates from each group.

Data Mining of the HTS Data Sets. The HTS data set was normalized using robust z-scores in order to minimize the influence of outliers and to account for the interplate variability.[55] Heat maps were developed from the normalized HTS data using the multi-experiment viewer (MeV) module in the TM4 microarray software suite.[56] Our HTS generated multidimensional data wherein the dimensionality was constituted by the type of NPs (7), dose (9), and durations of exposure (8), cellular targets (2), and cytotoxicity events (4). We utilized the self-organizing map (SOM) feature to visualize the relationships between NPs in their cytotoxicity profile and between cell lines in their response to NPs in the context of the HTS assay. SOMs were developed from the entire HTS data set using MATLAB in conjunction with the SOM Toolbox 2.0 software library. Briefly, the SOM algorithm performs a topology-preserving mapping from a high-dimensional input space onto a lower dimensional output space formed by a regular 2D grid of map units. During this process, SOM units are iteratively adapted to the underlying structure of the HTS data set. The main advantage of using SOM for exploratory data analysis is that the algorithm combines data clustering (*i.e.*, data quantization) with a topology preserving projection (*i.e.*, topological ordering) that results in the visualization of the "true" high-dimensional structure of the data set. This is because in the course of map construction process the location of SOM units adapts such that map units of greater similarity are organized closer to each other. Since the spatial relationships of each NP with respect to each other or cytotoxicity event in a SOM grid define their degree of similarity, SOM extends simple hierarchical clustering and allows easier interpretation of clustering results.[57,58] For example, NPs that elicit similar cytotoxicity events cluster together in the SOM grid (Figure 4a). A detailed description on the development of SOM and its application to HTS data analysis can be found in our manuscript in press.[58]

Zebrafish Embryo Exposure to NPs. Working NP solutions containing 1, 5, 15, and 25 ppm of each material were prepared in Holtfreter's medium as detailed above. Zebrafish embryos were collected in Holtfreter's medium 2 h post-fertilization (hpf) from mating cages. Embryos were visually assessed for quality, and the healthiest specimens were transferred into 96-well plates containing 1 embryo per well. Beginning at 4 hpf, the sphere stage of the embryo was exposed to 100 μL/well of NPs in Holtfreter's medium or a control solution without NPs. The Hotfreter's medium (containing NP) was exchanged daily up to 120 hpf. Three replicate trials that involve 12 embryos per

treatment group for 120 hpf were performed. The change in basal cardiac rate was assessed at 72 hpf, while the embryo hatching, survival, and morphological defects were assessed at 24, 48, 72, 96, and 120 hpf. Hatching rate was expressed as the number of embryos that were completely hatched by 72 hpf, while the mortality rate was expressed as the total number of dead embryos, 120 hpf. Screening for morphological defects included looking for pericardial/yolk sac edema, body length, large/small yolk, opaque yolk, short tail, and bent spine. Embryos exhibiting abnormal features were mounted in methyl cellulose and photographed to measure the length of the embryos and to capture images of the abnormal morphology. The injury impact was scored according to a scale of 0−4 based on the number of morphological and/or physiological defects, based on a scoring system described by Fako and Furgeson.[20] According to this scale, 0 corresponds to no defects, 1 to a single defect, 2 to a pair of defects, 3 to 3 or more defects, and 4 for lethality or failure to hatch by the end of the observation period. Each NP was tested using 12 embryos in triplicate for each assessment.

Acknowledgment. This work is supported by the National Science Foundation and the Environmental Protection Agency under Cooperative Agreement Number DBI 0830117. Any opinions, findings, conclusions or recommendations expressed herein are those of the author(s) and do not necessarily reflect the views of the National Science Foundation or the Environmental Protection Agency. This work has not been subjected to an EPA peer and policy review. Key support was provided by the U.S. Public Health Service Grants U19 ES019528 (UCLA Center for NanoBiology and Predictive Toxicology), RO1 ES016746, and RC2 ES018766. S.G. acknowledges Dr Armando Durazo, Molecular Instrumentation Center, University of California, Los Angeles, for the ICP-MS analysis.

Supporting Information Available: List and source of NPs used in the study, the properties and utilities of fluorescence probes used in this study, schematic for suspending NPs in cell culture and Holtfreter's medium, kinetics of NP agglomeration in mammalian tissue culture media, the layout of 384-well plate and use of fluorescence dyes to perform HTS analysis, correlation matrix for assessing the degree of correlation between different cytotoxicity parameters, NP agglomeration kinetics to show the stabilizing effect of alginate added to Holtfreter's medium, zebrafish embryo cardiac rate, zebrafish embryo toxicity to QD2 and QD3, HTS and ICP-MS analysis to show that Pt ions may contribute to nano-Pt toxicity. This material is available free of charge *via* the Internet at http://pubs.acs.org.

REFERENCES AND NOTES

1. Nel, A.; Xia, T.; Madler, L.; Li, N. Toxic Potential of Materials at the Nanolevel. *Science* **2006,** *311*, 622–627.
2. Nanotechnology Consumer Product Inventory. Washington DC: Project on Emerging Nanotechnology. Woodrow Wilson International Center for Scholars. Available at http://www.nanotechproject.org/inventories/consumer/.
3. Service, R. F. Nanotechnology—Can High-Speed Tests Sort out which Nanomaterials Are Safe? *Science* **2008,** *321*, 1036–1037.
4. Hartung, T. Toxicology for the Twenty-First Century. *Nature* **2009,** *460*, 208–212.
5. Council., N. R. *Toxicity Testing in the 21st Century: A Vision and a Strategy*; National Academy Press: Washington, DC, 2007.
6. George, S.; Pokhrel, S.; Xia, T.; Gilbert, B.; Ji, Z.; Schowalter, M.; Rosenauer, A.; Damoiseaux, R.; Bradley, K. A.; Mädler, L.; *et al.* Use of a Rapid Cytotoxicity Screening Approach To Engineer a Safer Zinc Oxide Nanoparticle through Iron Doping. *ACS Nano* **2010,** *4*, 15–29.
7. Kahru, A.; Dubourguier, H.-C. From Ecotoxicology to Nanoecotoxicology. *Toxicology* **2010,** *269*, 105–119.
8. Ofek, B.-I.; Ralph, M. A.; Valerie, E. F.; Darin, Y. F. Toxicity Assessments of Multisized Gold and Silver Nanoparticles in Zebrafish Embryos. *Small* **2009,** *5*, 1897–1910.
9. Asharani, P. V.; Wu, Y.; Gong, Z.; Valiyaveettil, S. Toxicity of Silver Nanoparticles in Zebrafish Models. *Nanotechnology* **2008,** *19*, 255102.
10. Pardo-Martin, C.; Chang, T.-Y.; Koo, B. K.; Gilleland, C. L.; Wasserman, S. C.; Yanik, M. F. High-Throughput *In Vivo* Vertebrate Screening. *Nat. Methods* **2010,** *7*, 634–636.
11. Lee, K. J.; Nallathamby, P. D.; Browning, L. M.; Osgood, C. J.; Xu, X.-H. N. *In Vivo* Imaging of Transport and Biocompatibility of Single Silver Nanoparticles in Early Development of Zebrafish Embryos. *ACS Nano* **2007,** *1*, 133–143.
12. Zhu, X.; Wang, J.; Zhang, X.; Chang, Y.; Chen, Y. The Impact of ZnO Nanoparticle Aggregates on the Embryonic Development of Zebrafish (*Danio rerio*). *Nanotechnology* **2009,** *20*, 195103.
13. King-Heiden, T. C.; Wiecinski, P. N.; Mangham, A. N.; Metz, K. M.; Nesbit, D.; Pedersen, J. A.; Hamers, R. J.; Heideman, W.; Peterson, R. E. Quantum Dot Nanotoxicity Assessment Using the Zebrafish Embryo. *Environ. Sci. Technol.* **2009,** *43*, 1605–1611.
14. Warheit, D. B.; Sayes, C. M.; Reed, K. L. Nanoscale and Fine Zinc Oxide Particles: Can *In Vitro* Assays Accurately Forecast Lung Hazards Following Inhalation Exposures? *Environ. Sci. Technol.* **2009,** *43*, 7939–7945.
15. Duffin, R.; Tran, L.; Brown, D.; Stone, V.; Donaldson, K. Proinflammogenic Effects of Low-Toxicity and Metal Nanoparticles *In Vivo* and *In Vitro*: Highlighting the Role of Particle Surface Area and Surface Reactivity. *Inhal. Toxicol.* **2007,** *19*, 849–856.
16. Rushton, E. K.; Jiang, J.; Leonard, S. S.; Eberly, S.; Castranova, V.; Biswas, P.; Elder, A.; Han, X.; Gelein, R.; Finkelstein, J.; *et al.* Concept of Assessing Nanoparticle Hazards Considering Nanoparticle Dosemetric and Chemical/Biological Response Metrics. *J. Toxicol. Environ. Health* **2010,** *73*, 445–461.
17. Ji, Z.; Jin, X.; George, S.; Xia, T.; Meng, H.; Wang, X.; Suarez, E.; Zhang, H.; Hoek, E. M. V.; Godwin, H.; *et al.* Dispersion and Stability Optimization of TiO_2 Nanoparticles in Cell Culture Media. *Environ. Sci. Technol.* **2010,** *44*, 7309–7314.
18. Xia, T.; Kovochich, M.; Liong, M.; Ma∧Dler, L.; Gilbert, B.; Shi, H.; Yeh, J. I.; Zink, J. I.; Nel, A. E. Comparison of the Mechanism of Toxicity of Zinc Oxide and Cerium Oxide Nanoparticles Based on Dissolution and Oxidative Stress Properties. *ACS Nano* **2008,** *2*, 2121–2134.
19. Xia, T.; Kovochich, M.; Liong, M.; Zink, J. I.; Nel, A. E. Cationic Polystyrene Nanosphere Toxicity Depends on Cell-Specific Endocytic and Mitochondrial Injury Pathways. *ACS Nano* **2008,** *2*, 85–96.
20. Xia, T.; Kovochich, M.; Brant, J.; Hotze, M.; Sempf, J.; Oberley, T.; Sioutas, C.; Yeh, J. I.; Wiesner, M. R.; Nel, A. E. Comparison of the Abilities of Ambient and Manufactured Nanoparticles To Induce Cellular Toxicity According to an Oxidative Stress Paradigm. *Nano Lett.* **2006,** *6*, 1794–1807.
21. Nel, A. E.; Mädler, L.; Velegol, D.; Xia, T.; Hoek, E. M. V.; Somasundaran, P.; Klaessig, F.; Castranova, V.; Thompson, M. Understanding Biophysicochemical Interactions at the Nano-Bio Interface. *Nat. Mater.* **2009,** *8*, 543–557.
22. Meng, H.; Xia, T.; George, S.; Nel, A. E. A Predictive Toxicological Paradigm for the Safety Assessment of Nanomaterials. *ACS Nano* **2009,** *3*, 1620–1627.
23. Fako, V. E.; Furgeson, D. Y. Zebrafish as a Correlative and Predictive Model for Assessing Biomaterial Nanotoxicity. *Adv. Drug Delivery Rev.* **2009,** *61*, 478–486.
24. Lamelas, C.; Wilkinson, K. J.; Slaveykova, V. I. Influence of the Composition of Natural Organic Matter on Pb Bioavailability to Microalgae. *Environ. Sci. Technol.* **2005,** *39*, 6109–6116.
25. Drake, P. L.; Hazelwood, K. J. Exposure-Related Health Effects of Silver and Silver Compounds: A Review. *Ann. Occup. Hyg.* **2005,** *49*, 575–585.
26. Orrenius, S.; Nicotera, P.; Zhivotovsky, B. Cell Death Mechanisms and Their Implications in Toxicology. *Toxicol. Sci.* **2010**Epub ahead of print.
27. Weber, H.; Roesner, J. P.; Nebe, B.; Rychly, J.; Werner, A.; Schröder, H.; Jonas, L.; Leitzmann, P.; Schneider, K. P.; Dummler, W. Increased Cytosolic Ca^{2+} Amplifies Oxygen Radical-Induced Alterations of the Ultrastructure and the Energy Metabolism of Isolated Rat Pancreatic Acinar Cells. *Digestion* **1998,** *59*, 175–185.

28. Rosenberg, N. L.; Spitz, M. C.; Filley, C. M.; Davis, K. A.; Schaumburg, H. H. Central Nervous System Effects of Chronic Toluene Abuse—Clinical, Brainstem Evoked Response and Magnetic Resonance Imaging Studies. *Neurotoxicol. Teratol.* **1988,** *10*, 489–495.
29. Mattia, C.; Ali, S.; Bondy, S. Toluene-Induced Oxidative Stress in Several Brain Regions and Other Organs. *Mol. Chem. Neuropathol.* **1993,** *18*, 313–328.
30. Mcdermott, C.; Allshire, A.; Van Pelt, F.; Heffron, J. J. A. Sub-Chronic Toxicity of Low Concentrations of Industrial Volatile Organic Pollutants *In Vitro*. *Toxicol. Appl. Pharmacol.* **2007,** *219*, 85–94.
31. Reedijk, J. New Clues for Platinum Antitumor Chemistry: Kinetically Controlled Metal Binding to DNA. *Proc. Natl. Acad. Sci. U.S.A.* **2003,** *100*, 3611–3616.
32. Pascoe, J. M.; Roberts, J. J. Interactions between Mammalian-Cell DNA and Inorganic Platinum Compounds. 1. DNA Interstrand Crosslinking and Cytotoxic Properties of Platinum(II) Compounds. *Biochem. Pharmacol.* **1974,** *23*, 1345–1357.
33. Elder, A.; Yang, H.; Gwiazda, R.; Teng, X.; Thurston, S.; He, H.; Oberdörster, G. Testing Nanomaterials of Unknown Toxicity: An Example Based On Platinum Nanoparticles of Different Shapes. *Adv. Mater.* **2007,** *19*, 3124–3129.
34. Zhang, L.; Cooper, A. J. L.; Krasnikov, B. F.; Xu, H.; Bubber, P.; Pinto, J. T.; Gibson, G. E.; Hanigan, M. H. Cisplatin-Induced Toxicity Is Associated with Platinum Deposition in Mouse Kidney Mitochondria *In Vivo* and with Selective Inactivation of the α-Ketoglutarate Dehydrogenase Complex in LLC-PK1 Cells. *Biochemistry* **2006,** *45*, 8959–8971.
35. Kirchner, C.; Liedl, T.; Kudera, S.; Pellegrino, T.; Muñoz Javier, A.; Gaub, H. E.; Stölzle, S.; Fertig, N.; Parak, W. J. Cytotoxicity of Colloidal CdSe and CdSe/ZnS Nanoparticles. *Nano Lett.* **2004,** *5*, 331–338.
36. Hardman, R. A Toxicologic Review of Quantum Dots: Toxicity Depends on Physicochemical and Environmental Factors. *Environ. Health Perspect.* **2006,** *114*, 165–172.
37. Derfus, A. M.; Chan, W. C. W.; Bhatia, S. N. Probing the Cytotoxicity of Semiconductor Quantum Dots. *Nano Lett.* **2003,** *4*, 11–18.
38. Müller, L. Consequences of Cadmium Toxicity in Rat Hepatocytes: Mitochondrial Dysfunction and Lipid Peroxidation. *Toxicology* **1986,** *40*, 285–295.
39. Ji, J. H.; Jung, J. H.; Kim, S. S.; Yoon, J. U.; Park, J. D.; Choi, B. S.; Chung, Y. H.; Kwon, I. H.; Jeong, J.; Han, B. S.;*et al.* Twenty-Eight-Day Inhalation Toxicity Study of Silver Nanoparticles in Sprague-Dawley Rats. *Inhal. Toxicol.* **2007,** *19*, 857–871.
40. Kim, Y. S.; Kim, J. S.; Cho, H. S.; Rha, D. S.; Kim, J. M.; Park, J. D.; Choi, B. S.; Lim, R.; Chang, H. K.; Chung, Y. H.;*et al.* Twenty-Eight-Day Oral Toxicity, Genotoxicity, and Gender-Related Tissue Distribution of Silver Nanoparticles in Sprague-Dawley Rats. *Inhal. Toxicol.* **2008,** *20*, 575–583.
41. Hussain, S. M.; Hess, K. L.; Gearhart, J. M.; Geiss, K. T.; Schlager, J. J. *In Vitro* Toxicity of Nanoparticles in Brl 3a Rat Liver Cells. *Toxicol. In Vitro* **2005,** *19*, 975–983.
42. Luckey, T. D.; Venugopal, B. Metal Toxicity in Mammals. In *Chemical Toxicology of Metals and Metalloids*; Venugopal, B., Luckey, T. D., Eds.; Plenum Press: New York, 1978; pp 32−36.
43. Bowman, T. V.; Zon, L. I. Swimming into the Future of Drug Discovery: *In Vivo* Chemical Screens in Zebrafish. *ACS Chem. Biol.* **2010,** *5*, 159–161.
44. Asharani, P. V.; Lianwu, Y.; Gong, Z.; Valiyaveettil, S. Comparison of the Toxicity of Silver, Gold and Platinum Nanoparticles in Developing Zebrafish Embryos. *Nanotoxicology* **2010**10.3109/17435390.2010.489207.
45. Hogstrand, C.; Wood, C. M. Towards a Better Understanding of the Bioavailability, Physiology and Toxicity of Silver in Fish: Implications for Water Quality Criteria. *Environ. Toxicol. Chem.* **1998,** *17*, 547–561.
46. Wesselkamper, S. C.; Chen, L. C.; Gordon, T. Development of Pulmonary Tolerance in Mice Exposed to Zinc Oxide Fumes. *Toxicol. Sci.* **2001,** *60*, 144–151.
47. Rohrs, L. C. Metal-Fume Fever from Inhaling Zinc Oxide. *Arch. Intern. Med.* **1957,** *100*, 44–49.
48. Xia, T.; Zhao, Y.; Sager, T.; George, S.; Pokhrel, S.; Li, N.; Schoenfeld, D.; Meng, H.; Lin, S.; Wang, X.;*et al.*Decreased Dissolution of ZnO by Iron Doping Yields Nanoparticles with Reduced Toxicity in the Rodent Lung and Zebra fish Embryos. *ACS Nano* **2011**, 10.1021/nn1028482.
49. Osterauer, R.; Haus, N.; Sures, B.; Köhler, H.-R. Uptake of Platinum by Zebrafish (*Danio rerio*) and Ramshorn Snail (*Marisa cornuarietis*) and Resulting Effects on Early Embryogenesis. *Chemosphere* **2009,** *77*, 975–982.
50. Kohonen, T. The Self-Organizing Map. *Proc. IEEE* **1990,** *78*, 1464–1480.
51. Yang, Z. R.; Chou, K.-C. Mining Biological Data Using Self-Organizing Map. *J. Chem. Inf. Comput. Sci.* **2003,** *43*, 1748–1753.
52. Thalamuthu, A.; Mukhopadhyay, I.; Zheng, X.; Tseng, G. C. Evaluation and Comparison of Gene Clustering Methods in Microarray Analysis. *Bioinformatics* **2006,** *22*, 2405–2412.
53. Dalton, L.; Ballarin, V.; Brun, M. Clustering Algorithms: On Learning, Validation, Performance, and Applications to Genomics. *Curr. Genomics* **2009,** *10*, 430–445.
54. Kroll, A.; Pillukat, M. H.; Hahn, D.; Schnekenburger, J. Current *In Vitro* Methods in Nanoparticle Risk Assessment: Limitations and Challenges. *Eur. J. Pharm. Biopharm.* **2009,** *72*, 370–377.
55. Daszykowski, M.; Kaczmarek, K.; Vander Heyden, Y.; Walczak, B. Robust Statistics in Data Analysis—A Review: Basic Concepts. *Chemom. Intell. Lab. Syst.* **2007,** *85*, 203–219.
56. Saeed, A. I.; Bhagabati, N. K.; Braisted, J. C.; Liang, W.; Sharov, V.; Howe, E. A.; Li, J.; Thiagarajan, M.; White, J. A.; Quackenbush, J. *et al.* Tm4 Microarray Software Suite. *Methods in Enzymology*; Academic Press: New York, 2006; Vol. 411, pp 134−193.
57. Vesanto, J., Hollmén, J. An Automated Report Generation Tool for the Data Understanding Phase. In *Hybrid Information Systems*; Abraham, A., Koppen, M., Eds.; Physica Verlag: Heidelberg, 2002; pp 611−626.
58. Rallo, R.; France, B.; Liu, R.; Nair, S.; Bradley, K.; Damoiseaux, R.; George, S.; Nel, A.; Giralt, F.; Cohen, Y. Self-Organizing Map Analysis of Toxicity-Related Cell Signaling Pathways for Metal and Metal Oxide Nanoparticles. *Environ. Sci. Technol.* **2011**10.1021/es103606x.